Nonlinear Processes in Geophysics (1999) 6: 169–178

Nonlinear Processes in Geophysics

Remarks on the parallel propagation of small-amplitude dispersive Alfvén waves

S. Champeaux[1], D. Laveder[2], T. Passot[2], and P. L. Sulem[2]

[1]Physics Department, University of California at San Diego, La Jolla, CA 92093-0319, USA
[2]CNRS, UMR 6529, Observatoire de la Côte d'Azur, B.P. 4229, 06304 Nice cedex 4, France

Received: 27 May 1999 – Revised: 20 September 1999 – Accepted: 28 September 1999

Abstract. The envelope formalism for the description of a small-amplitude parallel-propagating Alfvén wave train is tested against direct numerical simulations of the Hall-MHD equations in one space dimension where kinetic effects are neglected. It turns out that the magnetosonic-wave dynamics departs from the adiabatic approximation not only near the resonance between the speed of sound and the Alfvén wave group velocity, but also when the speed of sound lies between the group and phase velocities of the Alfvén wave. The modulational instability then does not anymore affect asymptotically large scales and strong nonlinear effects can develop even in the absence of the decay instability.

When the Hall-MHD equations are considered in the long-wavelength limit, the weakly nonlinear dynamics is accurately reproduced by the derivative nonlinear Schrödinger equation on the expected time scale, provided no decay instabilities are present. The stronger nonlinear regime which develops at later time is captured by including the coupling to the nonlinear dynamics of the magnetosonic waves.

1 Introduction

Due to the considerable complexity of the multidimensional MHD equations for both analytic developments and numerical simulations, strong interest has been paid to asymptotic equations that provide simplified descriptions in specific limits. When the Hall effect is taken into account in the generalized Ohm's law, the system is dispersive and the dynamics of weakly nonlinear waves is amenable to two different asymptotics. When the dispersion is kept finite, the modulation of a monochromatic wave with a small (but finite) amplitude is governed by a nonlinear Schrödinger equation for the complex amplitude of the wave with, in some instance, a coupling to low-frequency fields driven by the modulation. Differently, long waves for which the dispersion is comparable to the nonlinearity are amenable to a reductive perturbative expansion. In the context of Alfvén waves propagating along an ambient magnetic field, due to the equality of the phase velocity of the Alfvén wave and of the speed of sound in the zero-dispersion limit, the latter asymptotics does not lead to the canonical Korteweg-de Vries equation (Segur, 1978) but to the so-called "derivative nonlinear Schrödinger" (DNLS) equation for the two components of the magnetic field transverse to the propagation. Both approaches concentrate on large-scale phenomena and neglect counterpropagating waves. The decay instability is in particular ignored.

In the present paper, the validity of the above asymptotic models is tested against direct numerical simulations of the Hall-MHD equations, with initial conditions in the form of a weakly perturbed monochromatic Alfvén wave, a regime where the dynamics is mostly prescribed by the linear instabilities. The evolution of a weakly perturbed large-amplitude plane wave was considered by Hoshino and Goldstein (1989). Here we concentrate on small-amplitude waves in order to prevent the rapid development of a fully turbulent regime and to enable the system to display, at least for a while, a weakly nonlinear evolution amenable to asymptotic analysis.

When dissipative processes are neglected, the Hall-MHD equations read

$$\partial_t \rho_M + \nabla \cdot (\rho_M \mathbf{u}) = 0 \tag{1}$$

$$\rho_M (\partial_t \mathbf{u} + \mathbf{u} \cdot \nabla \mathbf{u}) = -\frac{\beta}{\gamma} \nabla \rho_M^\gamma + (\nabla \times \mathbf{b}) \times \mathbf{b} \tag{2}$$

$$\partial_t \mathbf{b} = \nabla \times (\mathbf{u} \times \mathbf{b}) - \frac{1}{R_i} \nabla \times \left(\frac{1}{\rho_M} (\nabla \times \mathbf{b}) \times \mathbf{b} \right) \tag{3}$$

$$\nabla \cdot \mathbf{b} = 0. \tag{4}$$

The equations are here written in non-dimensional units, where the Alfvén velocity is taken as unity, R_i denotes

Correspondence to: P.L. Sulem (sulem@obs-nice.fr)

the non-dimensional ion-cyclotron frequency and γ the polytropic gas constant. The parameter β (assumed to be finite) is the squared ratio of the sonic to the Alfvén speed. Assuming a uniform background magnetic field along the x-axis and variations of the fields in this direction only, Eqs. (1)–(4) reduce to

$$\partial_t \rho_M + \partial_x(\rho_M u_x) = 0 \tag{5}$$

$$\partial_t u_x + u_x \partial_x u_x = -\frac{1}{\rho_M}\partial_x\Big(\frac{\beta}{\gamma}\rho_M^\gamma + \frac{1}{2}|b|^2\Big) \tag{6}$$

$$\rho_M(\partial_t v + u_x \partial_x v) = \partial_x b \tag{7}$$

$$\partial_t b + \partial_x(u_x b - v) = i\frac{\sigma}{R_i}\partial_x\Big(\frac{1}{\rho_M}\partial_x b\Big) \tag{8}$$

where we introduced the complex notation $b = b_y - i\sigma b_z$ and $v = u_y - i\sigma u_z$, with either $\sigma = 1$ or $\sigma = -1$. The longitudinal component b_x remains constant and can be absorbed in the ambient field, taken as unity.

Equations (5)–(8) admit exact solutions in the form of monochromatic circularly polarized Alfvén waves $b = -(\omega/k)v = B_0 e^{i(kx-\omega t)}$, $u_x = 0$, $\rho_M = 1$. Keeping $k > 0$, the frequency ω of a forward-propagating wave obeys the dispersion relation $\omega = \frac{\sigma}{2R_i}k^2 + k\sqrt{1 + \frac{k^2}{4R_i^2}}$ where the choices $\sigma = 1$ or $\sigma = -1$ correspond to a right-hand or left-hand circularly polarized wave respectively.

2 Envelope dynamics

2.1 Modulation equations

The envelope equations governing the slow modulation of an Alfvén wave with a small (but finite) amplitude is obtained by a standard multiple-scale analysis (Champeaux et al., 1997). Defining the slow variables $X = \epsilon x$ and $T = \epsilon t$ and expanding

$$v = \epsilon v_1 + \epsilon^2 v_2 + \epsilon^3 v_3 + \cdots,\ b = \epsilon b_1 + \epsilon^2 b_2 + \epsilon^3 b_3 + \cdots,$$
$$\rho_M = 1 + \epsilon^2\rho_2 + \epsilon^3\rho_3 + \cdots,\ u_x = \epsilon^2 u_2 + \epsilon^3 u_3 + \cdots,$$

Eqs. (5)–(8) yield to leading order

$$\partial_t v_1 - \partial_x b_1 = 0, \qquad \partial_t b_1 - \partial_x v_1 - i\frac{\sigma}{R_i}\partial_{xx} b_1 = 0. \tag{9}$$

The solution of Eq. (9) corresponds to a circularly polarized Alfvén wave $b_1 = -(\omega/k)v_1 = B_1 e^{i(kx-\omega t)}$ whose complex amplitude now depends on the slow variables.

Elimination of the secular oscillating terms in the equations at order ϵ^2 for the transverse fields leads to

$$\partial_T B_1 + v_g \partial_X B_1 = 0 \tag{10}$$

which expresses that B_1 is advected at the group velocity $v_g \equiv \omega' = \frac{2\omega^3}{k(k^2+\omega^2)}$. At order ϵ^3, the solvability condition of the equations for the transverse fields reads

$$i(\partial_T B_2 + v_g \partial_X B_2) + \mathcal{D}B_1 - k(\bar{u}_{x_2} - \frac{v_g}{2}\bar{\rho}_2)B_1 = 0 \tag{11}$$

where we introduced the dispersion operator

$$\mathcal{D} = \frac{\omega}{\omega^2 + k^2}\Big(\frac{\omega^2}{k^2}\partial_{XX} + \frac{2k}{\omega}\partial_{XT} + \frac{k^2}{\omega^2}\partial_{TT}\Big). \tag{12}$$

From Eq. (10), $\mathcal{D}B_1 = \frac{\omega''}{2}\partial_{XX}B_1$. Furthermore, overbars denote averaging over the fast variables.

Writing the equations obeyed by $\bar{u}_{x_2}$ and $\bar{\rho}_2$, and defining $B = B_1 + \epsilon B_2$ one gets, after dropping overbars and subscripts,

$$i(\partial_T + v_g\partial_X)B + \epsilon\frac{\omega''}{2}\partial_{XX}B - \epsilon k\Big(u - \frac{v_g}{2}\rho\Big)B = 0 \tag{13}$$

$$\partial_T\rho + \partial_X u = 0 \tag{14}$$

$$\partial_T u + \partial_X\Big(\beta\rho + \frac{1}{2}|B|^2\Big) = 0. \tag{15}$$

In the long-wavelength limit $k \to 0$, this system reduces to that introduced by Ovenden et al. (1983).

In the frame moving at the Alfvén-wave group velocity the above system rewrites, in terms of the coordinate $\xi = X - v_g T$ and of the slower time $\tau = \epsilon T = \epsilon^2 t$

$$i\partial_\tau B + \frac{\omega''}{2}\partial_{\xi\xi}B - k\Big(u - \frac{v_g}{2}\rho\Big)B = 0 \tag{16}$$

$$\epsilon\partial_\tau\rho + \partial_\xi(u - v_g\rho) = 0 \tag{17}$$

$$\epsilon\partial_\tau u + \partial_\xi\Big(\beta\rho - v_g u + \frac{1}{2}|B|^2\Big) = 0. \tag{18}$$

Neglecting the terms of order ϵ in Eqs. (17)–(18) make ρ and u slaved to the magnetic field amplitude, in the form $u = v_g\rho = \frac{v_g|B|^2}{2(v_g^2-\beta)}$, (up to a constant in the periodic case). The long-wavelength modulation of the Alfvén wave envelope then obeys the nonlinear Schrödinger equation (NLS)

$$i\partial_\tau B + \frac{\omega''}{2}\partial_{\xi\xi}B + \frac{kv_g}{4(\beta - v_g^2)}|B|^2 B = 0. \tag{19}$$

This adiabatic approximation (also called static by Spangler (1987) in the context of the DNLS equation) clearly breaks down near the resonance $\beta = v_g^2$, associated with the equality between the group velocity of the Alfvén wave and the speed of sound. Near this resonance, Eqs. (16)–(18) simplify through an additional rescaling. Keeping unchanged the magnitude of the transverse velocity and magnetic field and defining $\beta^{1/2} - v_g = \epsilon^{2/3}\lambda$, $\xi = \epsilon^{2/3}(x - v_g t)$, $\tau = \epsilon^{4/3}t$, and $u_x - \frac{v_g}{2}(\rho_M - 1) = \epsilon^{4/3}\phi$, one gets the Hamiltonian system derived by Benney (1977) in a general context

$$i\partial_\tau B + \frac{\omega''}{2}\partial_{\xi\xi}B - k\phi B = 0 \tag{20}$$

$$\partial_\tau\phi + \lambda\partial_\xi\phi = -\frac{1}{8}\partial_\xi|B|^2. \tag{21}$$

Far from the resonance, a Hamiltonian formulation that differs from Eqs. (16)–(18) by subdominant terms only can also be given. Using the canonical variables $\tilde{u} = u - \Big(k + \frac{v_g}{2}\frac{kv_g - 1}{\beta - v_g^2}\Big)|B|^2$ and $\tilde{\rho} = \rho - \frac{kv_g - 1}{2(\beta - v_g^2)}|B|^2$, the

system takes the form of the equations introduced by Zakharov and Rubenchik (1972) for the interaction of high-frequency with low-frequency waves (see also Zakharov and Schulman (1991))

$$i\partial_\tau B + \frac{\omega''}{2}\partial_{\xi\xi}B - k\left(\tilde{u} - \frac{v_g}{2}\tilde{\rho} + q|B|^2\right)B = 0 \qquad (22)$$

$$\epsilon\partial_\tau\tilde{\rho} + \partial_\xi(\tilde{u} - v_g\tilde{\rho}) = -k\partial_\xi|B|^2 \qquad (23)$$

$$\epsilon\partial_\tau\tilde{u} + \partial_\xi(\beta\tilde{\rho} - v_g\tilde{u}) = \frac{kv_g}{2}\partial_\xi|B|^2. \qquad (24)$$

where $q = k + \frac{v_g}{4}\frac{kv_g-1}{\beta-v_g^2}$. Note that in contrast with Eqs. (16)–(18), this formulation becomes singular at the resonance.

2.2 Linear stability analysis

The NLS equation (19) admits a solution with a constant amplitude B_0 and a phase that is uniform in space and linear in time. At the level of the primitive equations, it corresponds to a monochromatic Alfvén wave whose frequency is slightly shifted by the nonlinearity. Linearization about this solution leads to the dispersion relation

$$\Omega^2 = \frac{\omega''^2}{4}K^4 - \frac{kv_g\omega''}{4(\beta - v_g^2)}B_0^2K^2, \qquad (25)$$

which predicts a long-wavelength modulational instability for $\beta > v_g^2$ or $\beta < v_g^2$ according to the right-hand ($\omega'' > 0$) or left-hand ($\omega'' < 0$) carrier polarization.

Linearization of the primitive MHD equations about an Alfvén wave of wavenumber k and amplitude b_0 (not restricted to be small), yields the dispersion relation

$$(\Omega^2 - \beta K^2)\mathcal{A}_+\mathcal{A}_- = \frac{b_0^2K^2}{2}(\mathcal{A}_+\mathcal{C}_- + \mathcal{A}_-\mathcal{C}_+) \qquad (26)$$

where

$$\mathcal{A}_\pm = (\omega \pm \Omega)^2 - (k \pm K)^2 - \frac{\sigma}{R_i}(\omega \pm \Omega)(k \pm K)^2$$

$$\mathcal{C}_\pm = -k(k \pm K) - \frac{\sigma}{R_i}k(\omega \pm \Omega)(k \pm K) + \frac{\Omega}{K}\left(\omega(k \pm K) + (\omega \pm \Omega)(k \pm K) - \frac{\sigma}{R_i}k^2(k \pm K)\right).$$

Following Wong and Goldstein (1986), the instability is said modulational when it affects wave numbers $K < k$ (not necessarily asymptotically small), and decay when $K > k$. Numerical resolution of the dispersion relation (26) for a carrier of small amplitude $b_0 \approx \epsilon B_0$ shows that for right-hand polarization the instability is modulational for $\beta > v_{ph}^2$ and of decay type for $\beta < v_{ph}^2$, where $v_{ph} = \omega/k$ is the phase velocity of the Alfvén wave. For left-hand polarization, the wave is stable for $\beta > v_{ph}^2$, while modulational and decay instabilities coexist for $\beta < v_{ph}^2$ (Fig. 1).

Figure 2 displays for different values of the parameter β the instability growth rate $\Im(\Omega(K))$ for a prescribed right-hand polarized carrying wave, as obtained from the primitive MHD equations and from envelope models. As often noted, such a polarization is predominant upstream of the Earth's bowshock. The primitive MHD equations show that the instability occurs at wave numbers $K = O(\epsilon)$ for $\beta > v_g^2$, as predicted by the NLS analysis (long-wavelength modulational instability). On the other side of the resonance $\beta = v_g^2$, the small K's are restabilized (an effect which, as noted by Longtin and Sonnerup (1986), is specific of small-amplitude waves) and the unstable modes are associated to wavenumbers

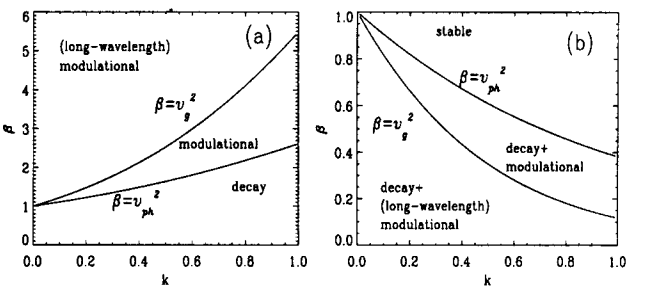

Fig. 1. Stability and instability regions in the plane (β, k) for small-amplitude Alfven waves with right-hand (a) or left-hand (b) polarization.

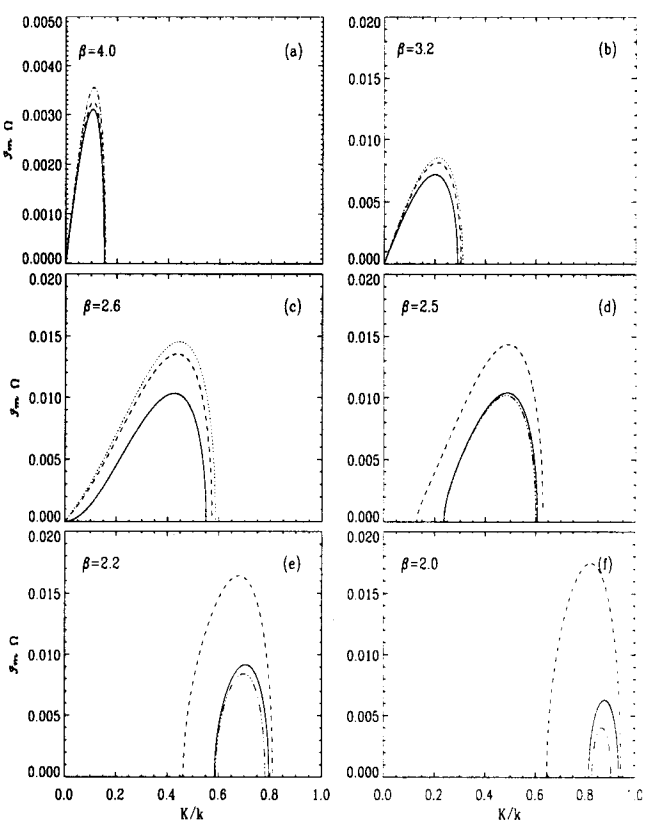

Fig. 2. Modulation instability growth rates for amplitude $\epsilon = 0.1$, $k = 0.64$ (corresponding to $v_g^2 = 3.20$ and $v_{ph}^2 = 1.81$) and right-hand polarization at various β, from the primitive MHD equations (solid line) and various envelope models: NLS equation (panel(a), dashed-dotted line), Eqs. (13)–(15) (dashed line), near-resonance model (20)–(21) (panels (b)-(c), dotted line), and improved model (33)–(35) (panels (d)–(f), dashed-dotted line).

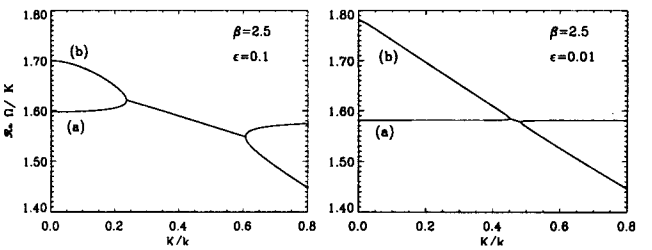

Fig. 3. Phase velocities of the perturbation modes from the primitive MHD equations with $\beta = 2.5$ and $k = 0.64$ ($v_g = 1.79$) for $\epsilon = 0.1$ (top) and $\epsilon = 0.01$ (bottom). The merging of the sonic branches (a) and the Alfvén branch (b) corresponds to the associated instability of Fig. 2(d) ($\epsilon = 0.1$).

K comparable to k (Wong and Goldstein, 1986). This transition is conveniently described by the reduced system (20)–(21), for which the dispersion relation reads

$$\Omega^3 - \lambda K \Omega^2 - \frac{\omega''^2}{4} K^4 \Omega - \frac{B_0^2 k \omega''^2}{8} K^3 + \frac{\lambda \omega''^2}{4} K^5 = 0. \quad (27)$$

From this equation, one easily shows that there exists $\lambda_c = \frac{3}{4} 2^{\frac{1}{3}} B_0^2 k |\omega''|$ such that the small-K modes are restabilized when $v_g - \beta^{1/2} > \epsilon^{2/3} \lambda_c$ (right-hand polarized wave) or $\beta^{1/2} - v_g > \epsilon^{2/3} \lambda_c$ (left-hand polarized wave), in agreement with the numerical observations on the primitive MHD equations.

Beyond the resonance $\beta = v_g^2$, the unstable wavenumbers remain finite as $\epsilon \to 0$, but the width of the unstable spectral band scales like ϵ. This is illustrated in Fig. 3, where the phase velocities $\Re(\Omega)/K$ of the modes that destabilize, computed from the primitive MHD equations, are displayed in the case $\beta = 2.5$ and $v_g^2 = 3.2$ for two different wave amplitudes ($\epsilon = 0.1$ and $\epsilon = 0.01$). The instability occurs when the phase velocity of an Alfvén branch originating from $\Re(\Omega)/K = v_g + O(\epsilon)$ as $K \to 0$ becomes equal to that of the acoustic mode $\Re(\Omega)/K \approx \beta^{1/2}$.

When β tends to v_{ph}^2, the unstable wave numbers approach the carrier wave number, while the maximum growth rate decreases and vanishes at $\beta = v_{ph}^2$. For $\beta < v_{ph}^2$, the decay instability develops and its growth rate rapidly increases as β gets smaller (Fig. 4).

Analogous results for left-hand polarized waves, for which modulational and decay instability branches coexist, are shown in Fig. 5.

The main observation is that the NLS equation which, as well known, cannot capture the decay instability, also misses the modulational instability that occurs in the region of the plane (β, k) between the two curves $\beta = v_g^2$ and $\beta = v_{ph}^2$. In this range of parameters, the unstable scales are too small to be accurately captured by the NLS asymptotics. In contrast, the dispersion relation for the envelope equations (13)–(15)

$$(\Omega^2 - \beta K^2)[4(\Omega - v_g K)^2 - \epsilon^2 \omega''^2 K^4] - \epsilon^2 B_0^2 \omega'' k K^3 (2\Omega - v_g K) = 0 \quad (28)$$

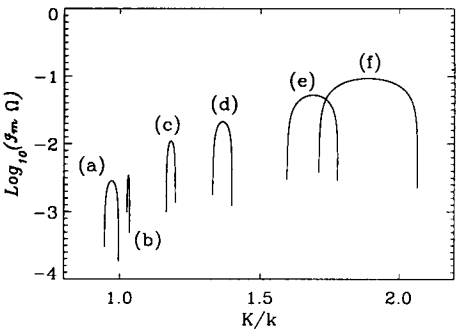

Fig. 4. Instability growth rates calculated on the primitive MHD equations for amplitude $\epsilon = 0.1$, $k = 0.64$ and right-hand polarization, showing the transition from modulational ((a), $\beta = 1.9$) to decay instability ((b), $\beta = 1.7$; (c), $\beta = 1.0$; (d), $\beta = 0.5$; (e), $\beta = 0.1$; (f), $\beta = 0.02$) in logarithmic scale.

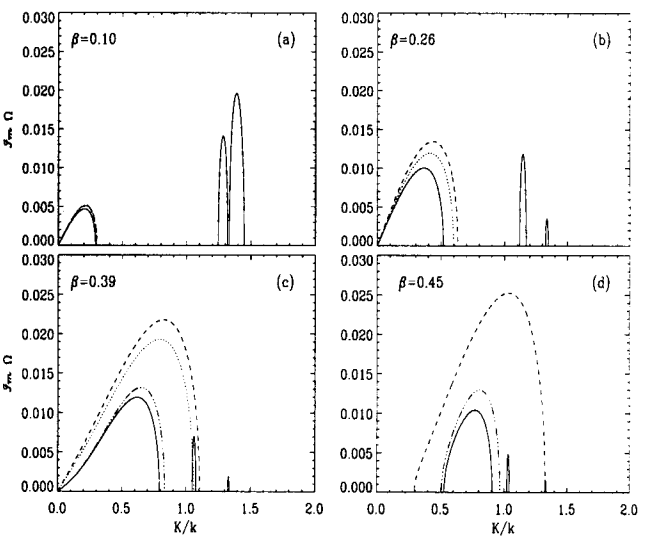

Fig. 5. Instability growth rates (modulational and decay) for amplitude $\epsilon = 0.1$, $k = 0.64$ (corresponding to $v_g^2 = 0.26$ and $v_{ph}^2 = 0.53$) and left-hand polarization at various β, for the primitive MHD equations (solid line), the NLS equation (panel(a), dashed-dotted line), the envelope equations (13)–(15) (dashed line), the near-resonance model (20)–(21) (panel (b)-(c), dotted line), and the higher-order envelope equations (33)–(35) (panels (c)-(d), dashed-dotted line).

predicts the persistence of the modulational instability for $\beta < v_g^2$ (right-hand polarization) or $\beta > v_g^2$ (left-hand polarization). Considering a perturbation with a wave number of order ϵ^{-1} given by $K = 2(v_g - \beta^{1/2})/(\epsilon \omega'') + Z$, and a phase velocity $\Omega/K = \beta^{1/2} + \epsilon Y$, the dispersion relation (28) asymptotically reduces to

$$Y^2 + \frac{\omega''}{2} ZY - B_0^2 k \omega'' \frac{v_g/2 - \beta^{1/2}}{8\beta^{1/2}(v_g - \beta^{1/2})} = 0. \quad (29)$$

According to this formula, a right-hand polarized wave ($\omega'' > 0$) is unstable when $v_g/2 < \beta^{1/2} < v_g$, while for left-hand polarization ($\omega'' < 0$) the instability occurs for $\beta^{1/2} < v_g/2$ or $\beta^{1/2} > v_g$. Assuming $v_g/2 < v_{ph}$ for right-hand polarization, which is usually verified in

the finite-dispersion regime, and concentrating on values of β between v_g^2 and v_{ph}^2, the present analysis reproduces the regimes sketched in Figs. 2(d–f) and 5(d). The quantitative predictions for the range of unstable wave numbers and for the growth rates become nevertheless poorly accurate when β approaches v_{ph}^2, due to the loss of scale separation between the carrier and the unstable modes in this regime. Furthermore, in the case of a right-hand polarized wave, the envelope equations (13)–(15) suffer from the existence of a spurious instability not present in the primitive MHD equations. For finite β, it arises in a small wave number band corresponding to scales significantly smaller than the carrier wavelength (by a factor 6 or 7), thus well outside of the range of validity of the asymptotics. These scales are nevertheless present in high-resolution simulations of the envelope equations, but the instability is conveniently removed by prescribing an adiabatic behavior for ρ and u at sufficiently small scales. This instability originates from the spurious crossing at large K of an Alfvén branch of phase velocity $\Re(\Omega)/K \approx v_g$ as $K \to 0$ with the acoustic mode $\Re(\Omega)/K \approx -\beta^{1/2}$, which should in fact remain stable for forward-propagating Alfvén waves. In the cold-plasma limit $\beta \to 0$, the spurious instability can affect the large scales. In this regime (where on the primitive equations the dynamics is in fact dominated by the decay instability) ρ and u are to be taken as slaved to the Alfvén-wave amplitude.

When considering (far from the resonance $\beta = v_g^2$) the accuracy of the Hamiltonian formulation (22)–(24) at the level of the linear stability analysis, the two polarizations must be distinguished. For right-hand polarized waves, the model leads to predictions similar to those of Eqs. (13)–(15), with the advantage that it does not suffer from a spurious small-scale instability. For left-hand polarization, in the range $\beta \ll v_g^2$ where on the primitive MHD equations decay and long-wavelength modulational instabilities coexist, the Hamiltonian model displays, in addition to a modulational instability, another instability at a wavenumber larger than that of the carrier, which results, in terms of the phase velocity, from the collision of an Alfvén branch with the acoustic branch that originates from $\beta^{1/2}$ at $K = 0$. As β approaches v_g^2, the two instabilities tend to merge and both disappear for $\beta > v_g^2$, in contrast with the primitive system. In the following, we thus abandon the use of Eqs. (22)–(24). The Hamiltonian structure does not indeed seem to play an important role in the present discussion concerning the evolution of perturbed plane wave, although it is essential in the context of the existence and stability theory of localized nonlinear waves.

2.3 Higher-order modulational analysis

The predictions of Eqs. (13)–(15) concerning the linear growth rate of the modulational instability when β approaches v_{ph}^2 can be refined by pushing the expansion to the next order in the modulational analysis of Sec. 2.1. Writing the solvability condition to eliminate secular oscillating modes, we get ($\mathcal{D}$ is defined in Eq. 12)

$$
\begin{aligned}
&i(\partial_T + v_g\partial_X)B_3 + \mathcal{D}B_2 \\
&\quad -i\frac{\omega}{\omega^2+k^2}\partial_T\Big(\frac{k}{\omega}\partial_T + \partial_X)^2 B_1 + i\partial_X((\bar{u}_2 - \frac{v_g}{2}\bar{\rho}_2)B_1\Big) \\
&\quad -k\Big((\bar{u}_2 - \frac{v_g}{2}\bar{\rho}_2)B_2 + (\bar{u}_3 - \frac{v_g}{2}\bar{\rho}_3)B_1\Big) \\
&\quad -i\frac{k^2}{\omega^2+k^2}\partial_T\Big((\bar{\rho}_2 - \frac{k}{\omega}\bar{u}_2)B_1\Big) + i\frac{k^3}{\omega(\omega^2+k^2)}\bar{u}_2\partial_T B_1 \\
&\quad +i\frac{\omega}{k^2+\omega^2}\Big(\frac{2k^2}{\omega}\bar{u}_2 - \frac{\omega^2}{k}\bar{\rho}_2\Big)\partial_X B_1 = 0. \qquad (30)
\end{aligned}
$$

The mean fields $\bar{u}_3$ and $\bar{\rho}_3$ satisfy

$$\partial_T\bar{\rho}_3 + \partial_X\bar{u}_3 = 0 \qquad (31)$$

$$\partial_T\bar{u}_3 + \partial_X(\beta\bar{\rho}_3 + B_1^*B_2 + B_2^*B_1) = 0 \qquad (32)$$

After straightforward substitutions, the equations obeyed by $B = B_1 + \epsilon B_2 + \epsilon^2 B_3$, $u = \bar{u}_2 + \epsilon\bar{u}_3$, $\rho = \bar{\rho}_2 + \epsilon\bar{\rho}_3$ take the form

$$
\begin{aligned}
&i(\partial_T + v_g\partial_X)B + \epsilon\Big(\frac{\omega''}{2}\partial_{XX} - i\epsilon\frac{\omega'''}{6}\partial_{XXX}\Big)B \\
&\quad +\epsilon(-k + i\epsilon\partial_X)\Big(u - \frac{v_g}{2}\rho)B\Big) \\
&\quad +i\epsilon^2\Big(-pB\partial_X(u - v_g\rho) + v_g(2p - \frac{1}{2})\rho\partial_X B\Big) = 0 \qquad (33)
\end{aligned}
$$

$$\partial_T\rho + \partial_X u = 0 \qquad (34)$$

$$\partial_T u + \partial_X\Big(\beta\rho + \frac{|B|^2}{2}\Big) = 0. \qquad (35)$$

with $p = \frac{k^2}{\omega^2+k^2}\Big(1 - \frac{kv_g}{2\omega}\Big)$ and

$$\omega''' = -\frac{6}{\omega^2+k^2}\Big(1 - \frac{kv_g}{\omega}\Big)\Big(v_g(1 - \frac{kv_g}{\omega}) + k\omega''\Big).$$

The associated dispersion relation is

$$
\begin{aligned}
&(\Omega^2 - \beta K^2)[4(\Omega - v_gK - \frac{\epsilon^2}{6}\omega'''K^3)^2 - \epsilon^2\omega''^2K^4] - \\
&4\epsilon^2B_0^2K^2[(1-p)\Omega + (p - \frac{1}{2})v_gK](\Omega - v_gK - \frac{\epsilon^2}{6}\omega'''K^3) \\
&-\epsilon^2B_0^2\omega''kK^3(2\Omega - v_gK) = 0. \qquad (36)
\end{aligned}
$$

The instability growth rate associated with this equation is also displayed in Fig. 2. The decrease of the growth rate as β approaches v_{ph}^2 is reproduced, even if the system restabilizes for a value of β slightly smaller than v_{ph}^2. Moreover, in this model, the previously mentioned spurious instability is suppressed. Note that the additional terms included in this model are of the same order in ϵ as those describing the deviation from adiabaticity in Eqs. (13)–(15). In contrast with these two models, the dispersion relation (36) coincides up to order ϵ^4 with the relation (26) derived from the primitive MHD equations. This results in a higher accuracy at the level of the linear theory. Equations (13)–(15)

should thus be viewed as models which supplement to the slow Alfvén wave modulation described by the NLS equation the lowest order coupling to the magnetosonic waves that evolve on a shorter time scale, without retaining other corrective terms arising at the same order of the expansion. This coupling is necessary to reveal the presence of a modulation type instability which for β between v_g^2 and v_{ph}^2 occurs at intermediate scales, the largest scales being stable.

2.4 Nonlinear dynamics

In order to study the nonlinear development of the previously discussed instabilities, pseudo-spectral simulations of the primitive MHD equations were performed in a periodic geometry, using as initial conditions a circularly polarized Alfvén wave perturbed by a small-amplitude random noise. Comparisons are presented with the predictions of the envelope equations (16)-(18). In all the simulations, the wave amplitude was taken equal to 10^{-1} and the magnitude of the noise of order 10^{-11}, so that the early time integration reproduces the linear phase. Both polarizations and various values of the parameter β were considered, for a wavenumber $k = 0.64$ corresponding to a group velocity $v_g = 1.79$ (right-hand polarization) or $v_g = 0.51$ (left-hand polarization). A dealiasing procedure was necessary in the regimes dominated by the long-wavelength instability.

2.4.1 Right-hand polarization

Simulations of the primitive MHD equations for $\beta = 4.0$, much in excess of the value $\beta \approx 3.2$ associated with the resonance $v_g = \beta^{1/2}$, show that in the nonlinear regime solitonic structures for the envelope of the transverse fields are formed (Fig. 6) and display a recurrent dynamics. Furthermore, as seen in Fig. 7, the density adiabatically follows the Alfvén wave intensity $\mathrm{b}^2 = b_y^2 + b_z^2$. As shown in Fig. 8, this dynamics is reproduced by the envelope equations (16)-(18), for which the adiabatic approximation is also verified. This model thus reduces to the NLS equation, which in periodic geometry leads to a recurrent behavior (Yuen and Ferguson, 1978). Note that, when normalized to the total elapsed time, the time difference between the snapshots of the direct simulation and of the model, presented in Fig. 8, is about 0.05, and thus consistent with the relative error of order $\epsilon = 0.1$ on the instability growth rates predicted by Eqs. (16)-(18).

Near the resonance, for $\beta = 3.2$, the magnetic field dynamics obtained from the primitive MHD equations is still of modulational type, and the envelope equations (16)-(18) provide a good approximation on the characteristic time scale, which near the resonance varies like $\epsilon^{-4/3}$ rather than the usual ϵ^{-2} (Fig. 9). As seen on Fig. 10, the density no longer follows the variations of the magnetic field amplitude. Eventually, strongly non-

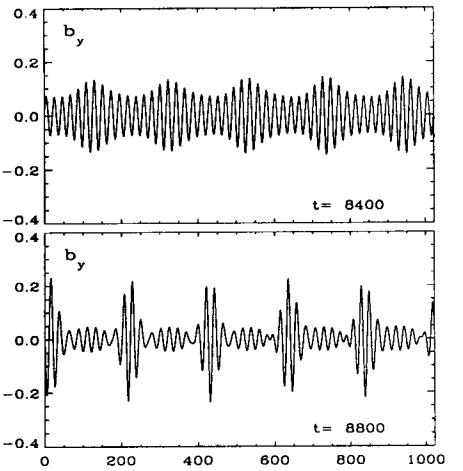

Fig. 6. Snapshots of the magnetic field b_y from the primitive MHD equations with $\beta = 4.0$, for an initially weakly perturbed right-hand polarized wave of amplitude $\epsilon = 0.1$ and $k = 0.64$.

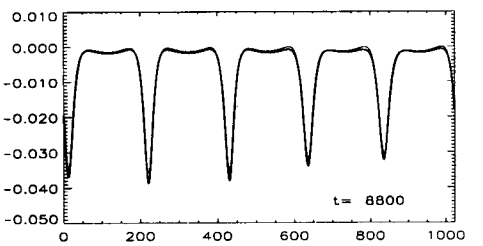

Fig. 7. Snapshot of the density ρ (corrected by a constant) from the primitive MHD equations (thick line) and the corresponding adiabatic prediction (thin line), for $\beta = 4.0$, amplitude $\epsilon = 0.1$, $k = 0.64$ and right-hand polarization.

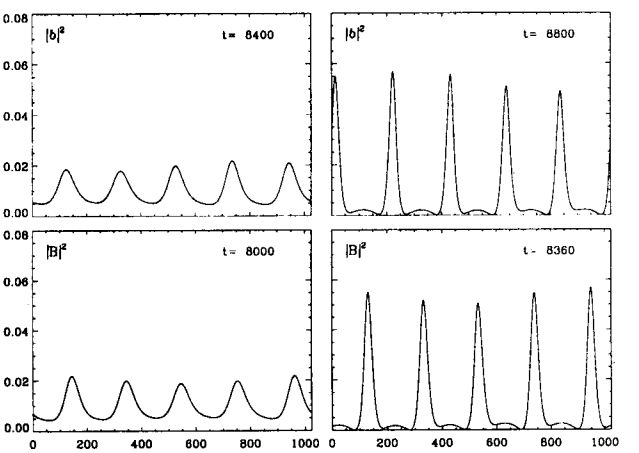

Fig. 8. Comparison of the squared Alfvén wave intensity obtained from the primitive MHD equations in the laboratory frame (top), and the envelope equations (16)-(18) in the Alfvén wave frame (bottom), for $\beta = 4.0$, amplitude $\epsilon = 0.1$, $k = 0.64$ and right-hand polarization at comparable times (see text).

linear effects develop on the primitive MHD equations, and a dissipative smoothing of viscous type is required in the simulation.

In the case $\beta = 2.45$, thus well beyond the resonance,

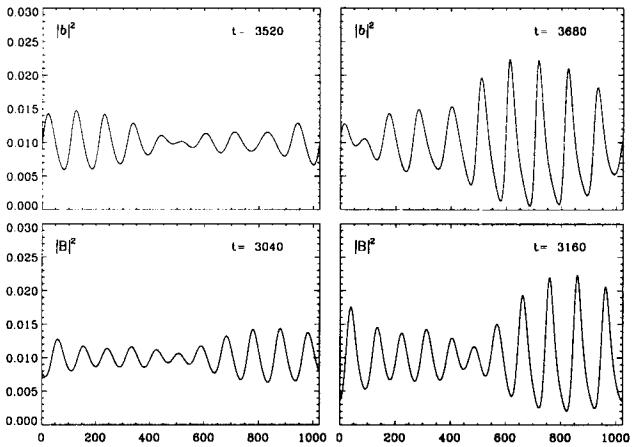

Fig. 9. Comparison of the squared Alfvén wave intensity obtained from the primitive MHD equations in the laboratory frame (top), and the envelope equations (16)–(18) in the Alfvén wave frame (bottom), for $\beta = 3.2$, amplitude $\epsilon = 0.1$, $k = 0.64$ and right-hand polarization at comparable times (see text).

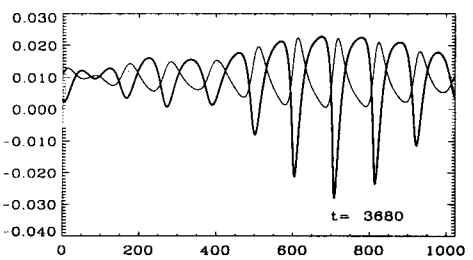

Fig. 10. Snapshot of the density ρ, corrected by a constant (thick line) and of the squared amplitude of the magnetic field $|\mathbf{b}|^2$ (thin line) obtained from the primitive MHD equations, for $\beta = 3.2$, amplitude $\epsilon = 0.1$, $k = 0.64$ and right-hand polarization.

the simulations of the MHD equations show that the dynamically relevant scales are not clearly separated from the carrier wavelength (Fig. 11). The envelope equations (16)–(18) can only provide a qualitative description of the dynamics, limited on a relatively short period of time. Even far from the resonance $v_g = \beta^{1/2}$, the adiabatic approximation does not hold and the MHD equations rapidly develop strong nonlinear phenomena, leading to density shocks (Fig. 11, where the small-scale oscillations are due to the Gibbs effect which develops in our non-dissipative code).

The question arises whether a better description of this regime could be provided by the higher-order system (33)–(35) that describes the linear phase very accurately. No significant improvement is in fact expected, mostly because this model does not include the nonlinear magnetosonic wave interactions that play an essential role in the long-time dynamics. Including these effects by pushing further the expansion would lead to a system whose numerical integration runs barely faster than the primitive equations, in a regime where the lack of scale separation strongly limits the accuracy of the envelope formalism.

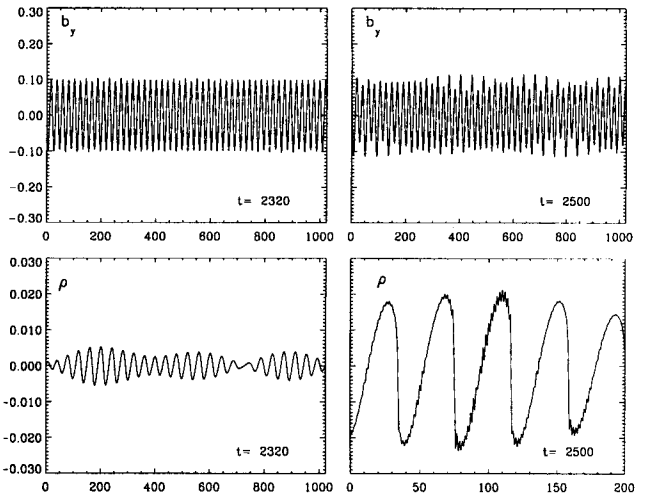

Fig. 11. Snapshots of the magnetic field b_y (top) and of the density ρ (bottom) obtained from the primitive MHD equations, for $\beta = 2.45$, amplitude $\epsilon = 0.1$, $k = 0.64$ and right-hand polarization. Shocks are showed on a magnified scale.

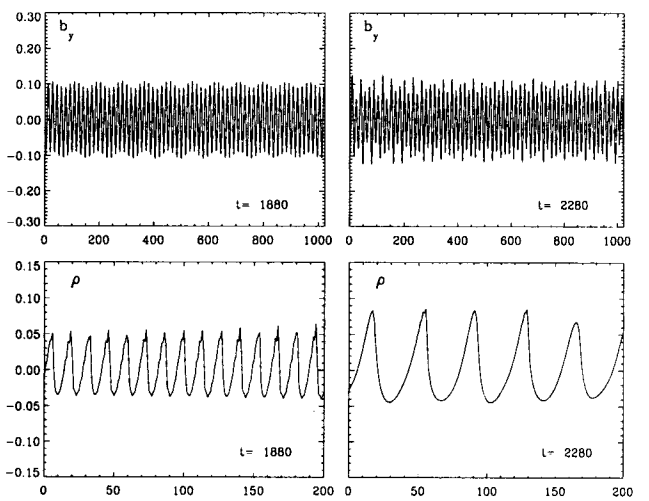

Fig. 12. Snapshots of the magnetic field b_y (top) and, on a magnified scale, of the density ρ (bottom) obtained from the primitive MHD equations with $\beta = 0.21$ (left) and $\beta = 0.30$ (right), for amplitude $\epsilon = 0.1$, $k = 0.64$ and left-hand polarization.

2.4.2 Left-hand polarization

As already mentioned, if the carrying wave is left-hand polarized, modulational and decay instabilities always coexist and the dynamics depends on the kind of instability that is prevalent. For a sufficiently small β the decay dominates the long-wavelength modulational instability (see Fig. 5), and strong nonlinearities rapidly develop, leading to small scales formation on the density field (Fig. 12, left). The modulational and decay growth rates become comparable when β slightly exceeds v_g^2. In this regime, the modulational instability affects scales that are not large enough to be accurately described by the envelope equations, and the corresponding evolution is seen in Fig. 12 (right). For larger β, the dynamics is

governed by a modulational instability at scales comparable to that of the carrier, and density shocks rapidly form.

3 Long-wavelength dynamics

3.1 The DNLS equation and its generalization

Consider the MHD equations (5-8) for $b = b_y + ib_z$ and $v = v_y + iv_z$. Define the stretched coordinate $\xi = \epsilon(x-t)$ and the slow time $\tau = \epsilon^2 t$, and also expand

$$v = \epsilon^{\frac{1}{2}}(v_1 + \epsilon v_2 + \cdots), \qquad b = \epsilon^{\frac{1}{2}}(b_1 + \epsilon b_2 + \cdots),$$
$$\rho_M = 1 + \epsilon\rho_1 + \epsilon^2\rho_2 + \cdots, \quad u_x = \epsilon u_1 + \epsilon^2 u_2 + \cdots.$$

At order $\epsilon^{3/2}$ one has $\partial_\xi(b_1+v_1) = 0$, and thus $b_1 = -v_1$. At order ϵ^2, one gets $u_1 = \rho_1 = \frac{|b_1|^2}{2(1-\beta)}$. At order $\epsilon^{5/2}$, the solvability condition for the equations governing the transverse fields then leads (writing b instead of b_1) to the DNLS equation

$$\partial_\tau b + \frac{i}{2R_i}\partial_{\xi\xi} b + \frac{1}{4(1-\beta)}\partial_\xi(|b|^2 b) = 0 \tag{37}$$

which is integrable by inverse scattering (Kaup and Newell, 1978). By pushing the expansion to higher order and retaining the own dynamics of magnetosonic waves (Passot and Sulem, 1995; Gazol et al., 1999) one gets (dropping again the subscript indices)

$$\partial_\tau b + \partial_\xi\left(\left(u - \frac{\rho}{2}\right)b\right) + \frac{i}{2R_i}\partial_{\xi\xi} b = 0 \tag{38}$$

$$\partial_\tau \rho + \partial_\xi(\rho u) + \frac{1}{\epsilon}\partial_\xi(u-\rho) = 0 \tag{39}$$

$$\partial_\tau u + \partial_\xi\left(\frac{u^2}{2} + \frac{\beta(\gamma-1)-1}{2}\rho^2\right) + \frac{1}{\epsilon}\partial_\xi\left(\beta\rho - u + \frac{|b|^2}{2}\right) = 0 \tag{40}$$

where the presence of the nonlinearities in the equations for ρ and u enables a uniform description of the resonance $\beta = 1$ (Hada, 1993). Kinetic effects are believed to be especially important in the latter regime, and can be modeled by means of a non-local additional term in the equation for the transverse field b (Mjølhus and Wyller, 1988; Spangler, 1990; Medvedev and Diamond, 1995). A related model (without these nonlinearities) was considered by Sakai and Sonnerup (1983) who concentrated on the linear stability. Comparisons with spacecraft observations are discussed by Spangler (1997).

3.2 Linear stability analysis

The DNLS equation also admits an exact solution in the form of circularly polarized Alfvén waves $b = b_0 e^{-i\sigma(k\xi-\omega\tau)}$ where, choosing $k > 0$, $\sigma = \pm 1$ for right-hand or left-hand polarization respectively. Linearization of the DNLS equation (37) about the above solution leads to the dispersion relation

$$\Omega^2 - 2K\left(\frac{\sigma k}{R_i} + \frac{b_0^2}{2(1-\beta)}\right)\Omega + \left(\frac{k^2}{R_i^2} - \frac{K^2}{4R_i^2} + \frac{3\sigma k b_0^2}{4R_i(1-\beta)} + \frac{3b_0^4}{16(1-\beta)^2}\right) = 0 \tag{41}$$

while the same analysis performed on Eqs. (38)-(40) yields

$$\left(\left(\Omega - \frac{\sigma k}{R_i}K\right)^2 - \frac{K^4}{4R_i^2}\right)\left((\epsilon\Omega + K)^2 - \beta K^2\right) - b_0^2 K^2\left(\epsilon\Omega + \frac{K}{2}\right)\left(\Omega - \frac{\sigma k}{2R_i}K\right) = 0. \tag{42}$$

Equation (41) predicts a modulational instability for right-hand (left-hand) polarized waves when $\beta > 1 + \frac{b_0^2 R_i}{4k}$ (respectively $\beta < 1 - \frac{b_0^2 R_i}{4k}$), which is also displayed by the numerical resolution of Eq. (42). In the limit of small amplitude b_0, this result reproduces the NLS prediction taken in the long-wavelength limit $k \to 0$. Note that because of the equality of the group and phase velocities in this limit, the modulational instability always affects the small wave numbers and is correctly captured by the adiabatic approximation.

On the primitive MHD equations, in the case of right-hand polarization, only the decay instability is present for $\beta < 1$. For $1 < \beta < 1 + \frac{b_0^2 R_i}{4k}$ the wave is stable, while for $\beta > 1 + \frac{b_0^2 R_i}{4k}$ it is modulationally unstable. In the case of left-hand polarization, modulational and decay instabilities coexist for $\beta < 1 - \frac{b_0^2 R_i}{4k}$, only the decay instability is present for $1 - \frac{b_0^2 R_i}{4k} < \beta < 1$ and the

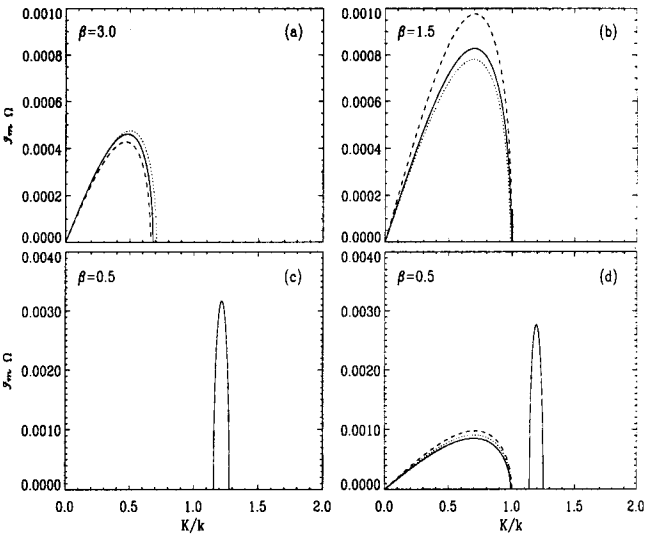

Fig. 13. Instability growth rates (modulational and decay) for amplitude $\epsilon^{1/2} = 0.25$, $k = \epsilon = 0.0625$ at various β for right-hand polarization (panels (a)–(c)) and left-hand polarization (panel (d)), from the primitive MHD equations (solid line), the DNLS equation (37) (dashed line) and the non-adiabatic DNLS model (38)–(40) (dotted line).

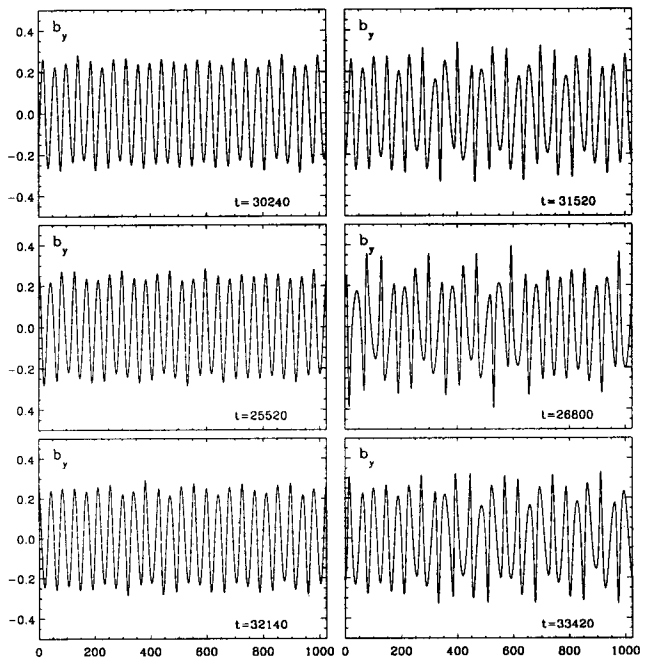

Fig. 14. Snapshots of the magnetic field b_y for $\beta = 1.5$, amplitude $\epsilon^{1/2} = 0.25$, $k = \epsilon = 0.0625$ and right-hand polarization, from the primitive MHD equations (top), the DNLS equation (medium), and the non-adiabatic DNLS system (bottom).

wave is stable for $\beta > 1$. The corresponding instability growth rates are shown on Fig. 13 for various values of β, together with the predictions of the DNLS models.

The non-adiabatic system (38)–(40) provides a better accuracy in predicting the modulational instability growth rates than the DNLS equation (37), especially when β approaches 1 (Fig. 13(b)). For $\beta < 0.25$, it however suffers from a spurious instability, similar to that affecting the envelope eqs. (13)–(15) and always localized at wavenumbers $K \gg k$ where the long-wavelength expansion is not expected to be accurate.

3.3 Nonlinear dynamics

In order to compare the DNLS models and the primitive MHD equations considered in the long-wavelength limit, simulations were performed using as initial conditions a circularly polarized monochromatic Alfvén wave, of amplitude $\epsilon^{1/2} = 0.25$ and wave number $\epsilon = 0.0625$, perturbed by a very weak random noise.

In the case of right-hand polarization, we used $\beta = 1.5$, for which only a modulational instability develops. For the primitive MHD equations, the linear phase saturates at a time ≈ 29000 while, due to the error on the instability growth rate, it saturates sooner for the DNLS equation (37) and later for its non-adiabatic generalization (38)–(40) (the normalized time shift being about 0.17 and 0.06 respectively). Figure 14 displays snapshots of the magnetic field, calculated from the MHD equations and the DNLS asymptotic models. For each

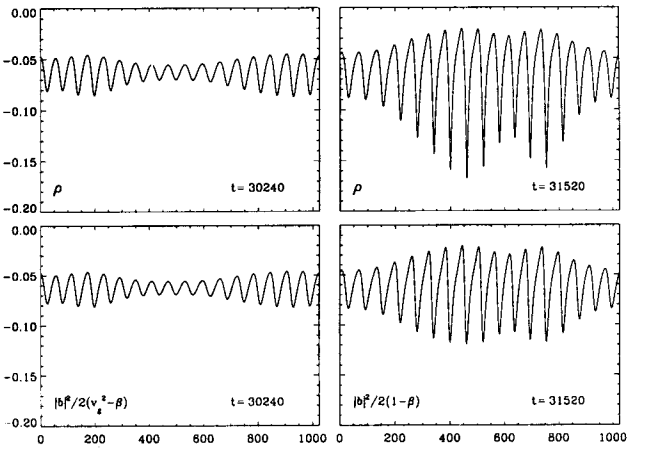

Fig. 15. Snapshots of the density ρ (corrected by a constant) from the primitive MHD equations (top) and the corresponding adiabatic prediction (bottom), for $\beta = 1.5$, amplitude $\epsilon^{1/2} = 0.25$, $k = \epsilon = 0.0625$ and right-hand polarization .

system, the snapshots are taken at times $t = t_0 + 5\epsilon^{-2}$ and $t_0 + 10\epsilon^{-2}$, where t_0 is the corresponding estimated time of the linear saturation and $5\epsilon^{-2} = 1280$. By comparing Figs. 14 (top) and 14 (medium), we note that the DNLS equation (37) well approximates the primitive system on a time scale $5\epsilon^{-2}$, while its accuracy begins to degrade after a time $10\epsilon^{-2}$, when the adiabaticity no longer holds and strongly nonlinear density cusp start to form (Fig. 15). On this time, the non-adiabatic system (38)–(40), which retains the essential nonlinear couplings between the fields, provides a better approximation of the MHD equations, as seen from a detailed inspection of Figs. 14 (top) and 14 (bottom).

Left-hand polarized Alfvén waves are stable for $\beta > 1$, therefore we investigate the case $\beta = 0.5$. Integration of the primitive MHD equations in this regime shows

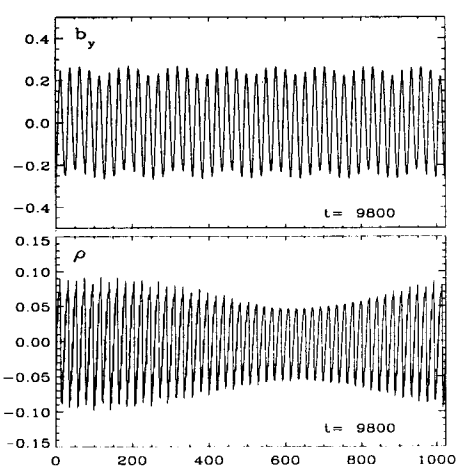

Fig. 16. Snapshots of the magnetic field b_y (top) and of the density ρ (bottom) obtained from the primitive MHD equations, for $\beta = 0.5$, amplitude $\epsilon^{1/2} = 0.25$, $k = \epsilon = 0.0625$ and left-hand polarization.

that the decay instability predominates over the modulational one and rapidly leads to a strongly nonlinear phase, with the formation of strong density gradients (Fig. 16).

4 Conclusion

Direct numerical simulations of parallel-propagating one-dimensional small-amplitude Alfvén wave trains were compared to the predictions of the envelope formalism and of DNLS-type equations in the small-dispersion regime. As well known, these asymptotic models do not retain backscattered Alfvén waves and thus ignore the decay instability which, when it coexists with the long-wavelength modulational instability, appears to be dominant. We note that a non-adiabatic dynamics for the density and longitudinal velocity is not restricted to the neighborhood of the resonance $v_g^2 = \beta$. The own dynamics of the magnetosonic waves is to be retained in order to capture the modulation type instabilities which develop for β between v_g^2 and v_{ph}^2 and affect scales comparable with that of the carrier, even when the amplitude of the latter is small. It is however important to stress that the present observations concern the evolution of a slightly perturbed plane wave. As discussed by Spangler et al. (1997), the strength of the decay instability could in particular be reduced in the case of a wave with a finite bandwidth. Other studies are to be performed to test the envelope formalism for a dispersive wave packet of finite extension and to analyze the predictions of the long-wavelength reductive perturbative expansion in the case of localized solutions. Of special interest is the quantitative characterization of the stability of a DNLS soliton when the parameter β is varied, a question initiated by Buti et al. (1998). Another point concerns situations where transverse perturbations are allowed (Viñas and Goldstein, 1991a,b). In the case of small-amplitude waves, the envelope formalism predicts a possible filamentation instability and the collapse of the Alfvén wave (Shukla and Stenflo, 1989), with the formation of sharp magnetosonic fronts (Champeaux et al., 1997). The influence of the decay instability in this regime is to be explored.

Acknowledgements. We thank M.L. Goldstein and M. Velli for useful discussions, and A. Noullez for providing the code used to solve the algebraic equations. This work was supported in part by "Programme National Soleil Terre" of CNRS.

References

Benney, D.J., A general theory for interactions between short and long waves, *Stud. Appl. Math.*, *56*, 81–94, 1977.

Buti, B., Jayanti, V., Viñas, A.F., Ghosh, S., Goldstein, M.L., Roberts, D.A., Lakhina, G.S., and Tsurutani, B.T., Nonlinear evolution of Alfvénic wave packets, *Geoph. Res. Lett.*, *25*, 2377–2379, 1998

Champeaux, S., Passot, T., and Sulem, P.L., Alfvén-wave filamentation, *J. Plasma Phys.*, *58*, 665–690, 1997.

Gazol, A., Passot, T., and Sulem, P.L., Coupling between nonlinear Alfvén waves and reduced magnetohydrodynamics for compressible fluids, *Phys. Plasmas*, *6*, 3114–3122, 1999.

Hada, T., Evolution of large amplitude Alfvén waves in the solar wind with $\beta \sim 1$, *Geophys. Res. Lett.*, *20*, 2415–2148, 1993.

Hoshino, M. and Goldstein, M.L., Time evolution from linear to nonlinear stages in magnetohydrodynamic parametric instabilities, *Phys. Fluids B*, *1*, 1405–1415, 1989

Kaup, D.J and Newell, A.C., An exact solution for the derivative nonlinear Schrödinger equation, *J. Math. Phys.*, *19*, 798–801, 1978.

Longtin, M. and Sonnerup, B.U.Ö., Modulation instability of circularly polarized Alfvén waves, *J. Geophys. Res.*, *91*, 6816–6824, 1986.

Mjølhus, E. and Wyller, J., Nonlinear Alfvén waves in a finite-beta plasma, *J. Plasma Phys*, *40*, 299–318, 1988.

Medvedev, M.V. and Diamond, P.H., Fluid models for kinetic effects on coherent nonlinear Alfvén waves. I. Fundamental theory, *Phys. Plasmas*, *3*, 863–873, 1995.

Ovenden, C.R., Shah, H.A., and Schwartz S.J., Alfvén solitons in the solar wind, *J. Geoph. Res.*, *88*, 6095–6101, 1983.

Passot, T. and Sulem, P.L., Nonlinear dynamics of dispersive Alfvén waves, in "Small-scale structures in three-dimensional hydrodynamics and magnetohydrodynamics turbulence" (M. Meneguzzi, A. Pouquet, and P.L. Sulem eds.,), *Lecture Notes in Physics*, *462*, 405–410, Springer Verlag, 1995.

Sakai, J.I. and Sonnerup, B.U.Ö., Modulational instability of finite amplitude dispersive Alfvén waves, *J. Geophys. Res.*, *88*, 9069–9079, 1983.

Segur, H., Solitons as Approximate descriptions of physical phenomena, *Rocky Mountain J. Math.*, *8*, 15–24, 1978.

Shukla, P.K. and Stenflo, L., Filamentation instability of Afven waves, *L., Astro. Space. Sci.*, *155*, 145-147, 1989

Spangler, S.R., Density fluctuations induced by nonlinear Alfvén waves, *Phys. Fluids*, *30*, 1104–1109,1987.

Spangler, S.R., Kinetic effects on Alfvén wave nonlinearity: The modified nonlinear wave equation, *Phys. Fluids B*, *2*, 407–418, 1990.

Spangler, S.R., Nonlinear evolution of MHD waves in the Earth bow shock: Opinions on the confrontation between theory, simulations and measurements, in "Nonlinear waves anc chaos in space plasmas", 171–224, T. Hada and H. Matsumoto eds., Terra Scientific Publishing Company (Tokyo), 1997.

Spangler, S.R., Leckband, J.A., and Cairns, I.H., Observations of the parametric decay instability of nonlinear magnetohydrodynamics waves, *Phys. Plasmas*, *4*, 846–855, 1997.

Viñas, A.F. and Goldstein, M.L., Parametric instabilities of circularly polarized large-amplitude dispersive Alfvén waves: excitation of parallel-propagating electromagnetic daughter waves, *J. Plasma Phys.*, *46*, 107–127, 1991.

Viñas, A.F. and Goldstein, M.L., Parametric instabilities of circularly polarized large-amplitude dispersive Alfvén waves: excitation of obliquely-propagating daughter and side-bands waves, *J. Plasma Phys.*, *46*, 129–152, 1991.

Wong, H.K. and Goldstein, M.L., Parametric instabilities of circularly polarized Alfvén waves including dispersion *J. Geophys. Res.*, *91*, 5617–5628, 1986.

Yuen, H.C. and Ferguson, W.E., Benjamin-Feir instability and recurrence in the nonlinear Schrödinger equation, *Phys. Fluids*, *21*, 1275–1278, 1978.

Zakharov, V.E. and Rubenchik, A.M., Nonlinear interaction between high and low frequency waves, *Prikl. Mat. Techn. Fiz.*, *5*, 84–98, 1972 (in Russian).

Zakharov, V.E. and Schulman, E.I, Integrability of nonlinear systems and perturbation theory, in "What is integrability ?", 185–250, V.E. Zakharov ed., Springer-Verlag, 1991.